

Seeing a Deep Ocean CO₂ Enrichment Experiment in a New Light: Laser Raman Detection of Dissolved CO₂ in Seawater

RACHEL M. DUNK, EDWARD T. PELTZER,
PETER M. WALZ, AND
PETER G. BREWER*

Monterey Bay Aquarium Research Institute,
7700 Sandholdt Road, Moss Landing, California 95039-9644

We used a newly developed in situ laser Raman spectrometer (LRS) for detection of elevated levels of dissolved CO₂ in seawater. The experiment was carried out at 500 m depth, 6 °C, to examine new protocols for detection of CO₂-enriched seawater emanating from a liquid CO₂ source in the ocean, and to determine current detection limits under field conditions. A system of two interconnected 5 L chambers was built, with flow between them controlled by a valve and pump system, and this unit was mounted on an ROV. The first chamber was fitted with a pH electrode and the optical probe of the LRS. In the second chamber ~580 mL of liquid CO₂ was introduced. Dissolution of CO₂ across the CO₂-seawater interface then occurred, the valves were opened, and a fixed volume of low-pH/CO₂-enriched seawater was transferred to the first chamber for combined pH/Raman sensing, where we estimate a mean dissolution rate of ~0.5 (μmol/cm²)/s. This sequence was repeated, resulting in measurement of a progressively CO₂ enriched seawater sample. The rapid in-growth of CO₂ was readily detected as the Fermi dyad of the dissolved state with a detection limit of ~10 mM with spectral acquisition times of 150 s. The detection of background levels of CO₂ species in seawater (~2.2 mM, dominantly HCO₃⁻) will require an improvement in instrument sensitivity by a factor of 5–10, which could be obtained by the use of a liquid core waveguide.

Introduction

The rapid development of laser Raman spectrometers (LRSs) for deep-sea science (1, 2) provides new opportunities for advanced sensing of chemical processes in the ocean, with applications to methane hydrates, hydrothermal vent minerals and fluids, and gas fractionation studies, all now in progress.

Raman detection of the oceanic CO₂ system (TCO₂ = CO₂(aq) + H₂CO₃ + HCO₃⁻ + CO₃²⁻) provides a particularly attractive target, with the unique promise of separate detection of the CO₂ system species, since each has a characteristic spectroscopic signal (3, 4). In an early deployment of a deep-sea LRS system, Brewer et al. (1) successfully acquired a Raman spectrum from a pool of liquid CO₂ on the seafloor at 3600 m depth. However, the natural levels of CO₂ in the ocean are typically too low ([TCO₂] ≈ 2–2.5 mM) to

detect with current instrument sensitivity. Nevertheless, there are significant opportunities for signal enhancement (5–7), and there are also occasions where strongly elevated CO₂ levels can occur. These can be either man-made, as with the ocean sequestration of CO₂ (8–10), or natural deep-sea volcanic sources, including both the direct venting of liquid CO₂ from the seafloor (11, 12) and hydrothermal vent sites, where end-member fluids typically have a [TCO₂] of 10–20 mM, and can reach a highly enriched [TCO₂] of 60–300 mM in back-arc or hot-spot locations (13).

Under CO₂-enriched conditions, the lowered seawater pH perturbs the normal partitioning of the oceanic CO₂ system (with HCO₃⁻ as the predominant species), and dissolved CO₂ (CO₂* = CO₂(aq) + H₂CO₃) becomes dominant. The deep ocean is a cold, high-pressure environment, and at low temperatures the hydration rate of CO₂ in seawater is slow (14, 15). A pH electrode senses only hydrogen ions, and thus will not detect the dissolved molecular CO₂ signal until after the hydration step, and subsequent rapid deprotonation steps, is complete. This can result in underestimation of the true dissolved CO₂ burden, and such an instance has been reported (10) where, close to a liquid CO₂ source at 3960 m depth, pH measurements greatly underestimated the near-field dissolved CO₂ signal, and corrections were made by observing the reduction in conductivity caused by the large quantity of nonionic species flowing by the sensor.

The ability to acquire in situ data allowing a direct quantitative assessment of carbonate speciation would present a powerful new tool to the oceanographic community, and this has attracted the attention of many researchers, with numerous studies on aqueous CO₂ and simple alkali-metal bicarbonate and carbonate solutions (4, 5, 16–18). Davis and Oliver (4) determined the molecular symmetry of aqueous CO₂, bicarbonate ion, and carbonate ion in relatively concentrated aqueous media (CO₂(g) at 5 atm in equilibrium with H₂O, and HCO₃⁻ and CO₃²⁻ at 0.2–8 M). The authors noted the appearance of a carbonate band in a KHCO₃ solution, and conducted a simple titration experiment that clearly demonstrated Raman detection of the shift in equilibrium position from the bicarbonate to carbonate ion as the pH increased. This study was followed by the first steps toward examination of the CO₂ system in natural waters, with analysis of more dilute solutions to a lower limit of 100 mM (16). More recently, Raman studies of the CO₂ system speciation in synthetic hydrothermal solutions (1 M HCO₃⁻ and CO₃²⁻, 22–550 °C, 100–200 dbar) have been used to investigate the accuracy of, and provide essential experimental data for, theoretical thermodynamic models of this complicated system (18). Although these studies have provided valuable fundamental information on the aqueous CO₂ system, no field applications have yet been carried out.

Information on the dissolution rate of liquid CO₂ in seawater at depth is also needed as input for the design of free ocean CO₂-enrichment (FOCE) experiments, in which it is envisioned that CO₂ is added to seawater in a controlled fashion to create a local environment that simulates the anticipated high-[CO₂]-low-pH characteristics of the ocean during the latter part of the 21st century (19, 20). Such a procedure is technically challenging, and will most likely require formation of a precursor CO₂-enriched fluid (of known concentration) within a reaction vessel under strictly controlled conditions, as opposed to simple injection of CO₂ into the FOCE control zone.

Here we present results of Raman detection of CO₂ dissolving into seawater at 500 m depth and 6 °C, and a determination of the current in situ detection limits. These

* Corresponding author phone: (831) 775-1706; fax: (831) 775-1620; e-mail: brpe@mbari.org.

may differ from laboratory detection limits due to the combined effects of pressure and temperature on the fully assembled sea-going spectrometer system. We also use pH measurements to estimate the dissolution rate of CO₂ into seawater within a dual-chamber reaction vessel designed to minimize hydrate formation during the production of CO₂-enriched seawater.

Experimental Section

Laser Raman System. We used the deep-ocean Raman in situ spectrometer (DORISS) (1, 2), with modifications as described by White et al. (21). DORISS is a laboratory model laser Raman spectrometer (LRS) from Kaiser Optical Systems, Inc. (KOSI), adapted for use in the deep sea to depths as great as 4000 m. The instrument consists of a 532 nm Nd:YAG laser, a holographically filtered probe head with interchangeable optics, a holographic duplex grating, and a 512 × 2048 front-illuminated CCD camera from Andor Technology. The duplex grating splits the spectrum into two stripes on the face of the CCD chip, providing a spectral range of 100–4400 Δcm⁻¹ with a digital resolution of ~1 Δcm⁻¹ per pixel. An immersion optic with an *f*/2 lens at the end of a 25 cm metal tube sealed with a sapphire pressure window (rated to 3000 psi) was used for this experiment. The working distance (from sapphire window to focal point) of this optic is 4 mm in seawater.

The spectrometer was calibrated on deck immediately prior to deployment, using a neon lamp for wavelength calibration, and a calibrated tungsten lamp for intensity. The laser wavelength was calibrated against the 801 Δcm⁻¹ Raman line of cyclohexane (22). A small diamond plate was placed inside the probe head in the laser beam path, so that the 1332 Δcm⁻¹ diamond Raman line is superimposed on all acquired spectra. This also provides a wavelength reference standard (1, 23). The full width at half-maximum (fwhm) height of the sharpest lines in the neon spectrum was ~3.7 Δcm⁻¹, giving a spectral resolution of ~4.6 cm⁻¹ (according to the Rayleigh criterion) for this deployment. The laser power output, measured at the focal point of the immersion optic prior to deployment, was ~28 mW. Spectra were acquired using KOSI's HoloGRAMS software, where dark spectrum subtraction and wavelength and intensity correction were performed by HoloGRAMS during acquisition and the processed spectra were saved in generic spectrum (.spc) format.

Apparatus. A system of two interconnected 4.95 L cylindrical acrylic chambers was built, with flow between them controlled by a valve and pump system (Figure 1). The internal volume of the associated valves and tubing was approximately 100 mL, giving a total system volume of ~10 L.

The first, or measurement, chamber was equipped with a thermistor for logging temperature and a pressure-balanced glass combination pH electrode (Ag/AgCl reference probe, Seabird Electronics, Inc., SBE-18), modified by the manufacturer to be deployed at depth. The output from the pH electrode is internally amplified and offset to yield an analogue output signal voltage between 0 and 5 V. The pH probes were calibrated using seawater solutions where the pH had been previously adjusted using concentrated HCl or NaOH to ~6 and ~8 as measured by an IQ240 ISFET pH electrode (IQ Scientific Instruments) that was calibrated using commercially available NBS pH standard solutions. The Raman immersion optic was inserted horizontally into this chamber, such that the focal point of the optic was positioned at the same height as the pH electrode tip and approximately in the center of the chamber volume.

The second, or dissolution, chamber was equipped with a thermistor at the base and the CO₂ inlet at the top. This chamber was also fitted with hydraulically controlled ports

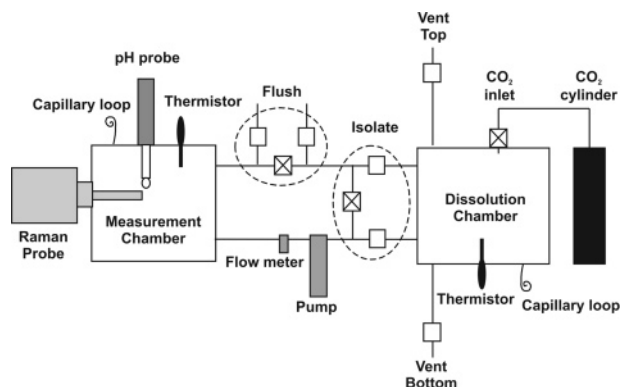


FIGURE 1. Schematic showing the experimental apparatus used for combined Raman and pH sensing of CO₂-enriched seawater at 500 m depth on the ROV *Ventana*. Squares represent hydraulically controlled valves (a square with “X” means the valve is closed). The flush and isolate valves each consist of three individual valves operated on the same hydraulic function. Valve positions are shown for deployment to allow flooding of the chambers with seawater during the ROV descent to 500 m.

for venting seawater (or CO₂) at both the top and bottom (“vent” valves). The liquid CO₂ was delivered from a 9 L accumulator mounted on the rear of *Ventana* following techniques described previously (9).

Ports entering and exiting from the sides of the acrylic chambers allowed circulation of seawater between the two chambers via nylon tubing (12.7 mm i.d.). A flow meter and Seabird 5T pump were positioned on the lower tubing path, such that the direction of pumped flow was from the lower port of the dissolution chamber to the lower port of the measurement chamber, with return flow above. The upper tubing path included a hydraulically controlled valve array (“flush” in Figure 1) to allow flushing of the system with ambient seawater. Another hydraulic valve array (“isolate” in Figure 1) between the upper and lower tubing paths allowed isolation of the dissolution chamber with continued circulation of fluid only through the measurement chamber. Both chambers were equipped with a capillary tube (0.5 mm i.d.), open to the ocean, to accommodate the volume changes.

The pH, thermistor, and flow sensor data were digitized and transmitted in real time via the ROV tether to the control room aboard the R/V *Point Lobos* and recorded.

Field Experiment. The experiment took place on May 9, 2005, at 500 m depth in Monterey Bay, CA, where the *P–T* environment ensured the liquid phase of CO₂ was within the CO₂ hydrate stability zone (8, 9). We used the ROV *Ventana* deployed by the RV *Point Lobos* as experimental platforms for equipment deployment and control. The DORISS probe-head pressure housing and the experimental apparatus were mounted on a rigid square bar across the front of the ROV, such that the apparatus was within the field of view of the main science camera on the ROV (Figure 2). Hydraulic actuation opened and closed the flush and isolate valve assemblies; both are shown in the open position in Figure 1. The viewing system on *Ventana* allowed for real-time observation of the experiment, providing visual confirmation of the CO₂ injection and hydraulic valve switching. All lights on the ROV were turned off while Raman spectra were collected; the light provided by the laser was sufficient to allow continued viewing of the experiment.

In our experience, the DORISS system shows some decrease in sensitivity in field deployments when compared to laboratory experiments, most easily recognized by a reduction in the total intensity (Raman peak area) of the water stretching band. This decrease in sensitivity is most likely due to the effect of pressure on the external fiber optic cables and to small changes in the optical path of the

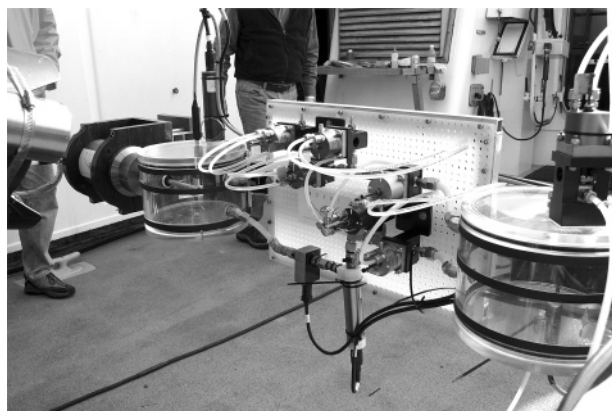


FIGURE 2. Experimental apparatus mounted on the front of the ROV *Ventana*. The Measurement chamber is to the left, with the Raman probe head supported by the two black rings. The valve assembly is at the center, with the pump and flow meter extending down from the lower loop. The dissolution chamber is at the right, with the CO₂ introduction valve mounted on top of the chamber.

spectrometer from both pressure- and temperature-induced stresses. In the experiment reported here, seawater spectra acquired during the ROV descent indicate no signal loss between 100 and 300 m, and a loss of ~20% at 500 m depth.

Procedure. The procedure was to dive the vehicle to 500 m water depth, with the pump on and the flush, isolate, and vent valves open to allow flooding of the apparatus. At 500 m the two vent valves were closed, and the apparatus was flushed with ambient seawater until the temperature measured in both chambers was equal to the external ocean value. The flush and isolate valves were then closed, the pump was turned off, and a spectrum of the ambient seawater contained inside the measurement chamber was collected. The bottom vent valve on the dissolution chamber was then opened to allow displacement of seawater, and 580 mL (4.5 strokes of a 128 mL piston) of liquid CO₂ was injected into the dissolution chamber. Immediately following injection, the bottom vent valve was closed. At 500 m, liquid CO₂ is buoyant with respect to seawater, and thus formed a layer at the top of the chamber. Dissolution of CO₂ across this interface creates seawater strongly enriched in dissolved inorganic carbon (DIC) within the dissolution chamber. The CO₂ was allowed to dissolve for ~10 min. The pump was then turned on, and the following series of steps were repeated 15 times: (a) the isolate valve assembly was opened, allowing CO₂-enriched seawater to circulate between the dissolution chamber and the measurement chamber; (b) the isolate valve assembly was closed, and the CO₂-enriched fluid was recirculated through the measurement chamber to ensure good mixing; (c) the pH in the measurement chamber was used to monitor mixing, where the pH decreases as the added CO₂-enriched water becomes well mixed and equilibrates with the water initially held in the measurement chamber; (d) once the pH approached a constant value, a Raman spectrum of the CO₂-enriched fluid was obtained. Throughout these steps, CO₂ is continuously dissolving across the CO₂-seawater interface within the dissolution chamber. During step a, this occurs under vigorous flow conditions, which disturbed the CO₂-seawater interface. For steps b–d, dissolution occurs under static no-flow conditions. The flow rate was logged continuously, and the time of all valve switching was recorded accurately; thus, the volume of water pumped between the chambers, and the timing of each step, is well-known. For samples 1–11, the isolate valve was held open for ~1 min, exchanging ~1350 mL of water between the chambers. For samples 12–15, this was increased to ~2 min, exchanging ~2700 mL of water. A Raman spectrum of each sample was obtained with a total acquisition time of

TABLE 1. Summary of the Valve Status during the Experiment Procedures

procedure	flush	isolate	vent top	vent bottom	CO ₂ inlet
flooding apparatus during descent	open	open	open	open	closed
flushing with ambient seawater	open	open	closed	closed	closed
injection of liquid CO ₂	closed	closed	closed	open	open
pumping between chambers	closed	open	closed	closed	closed
recirculating in measurement chamber	closed	closed	closed	closed	closed

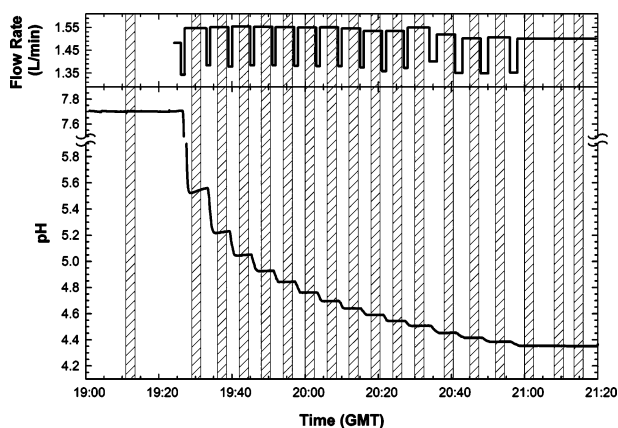


FIGURE 3. Flow meter and pH data over the course of the experiment. The vertical gray bars indicate the time of spectral acquisition. When the isolate valve is closed, a high flow rate of ~1.55 L/min is observed. When the isolate valve is open, a lower flow rate of ~1.35 L/min is observed.

150 s. The short time step between each sample point (chosen to allow clear observation of the in-growth of the CO₂ signal) did not permit replicate measurements to be made. However, at the end of the experiment triplicate measurements were made of the final sample S15, enabling an estimate of the instrument precision to be made.

The valve positions for all experimental procedures are summarized in Table 1. The logged flow meter and pH data, and the time of spectral acquisitions, are shown in Figure 3.

Results and Discussion

pH Signal. The raw sensor (electrode + preamplifier) output voltage obtained was converted to pH using the equation

$$\text{pH} = 7 + (V_{\text{out}} - \text{offset}) / (KT(\text{slope})) \quad (1)$$

where V_{out} is the pH electrode output voltage, $K = (R/F) \ln 10$, R is the gas constant ($8.3144 \text{ K}^{-1} \text{ mol}^{-1}$), F is the Faraday constant ($9.6485 \times 10^4 \text{ C mol}^{-1}$), and T is temperature in degrees kelvin.

The evolution of pH in the Raman chamber over the duration of the experiment is shown in Figure 3, and the average pH measured across each spectral acquisition is given in Table 2. The [TCO₂] and CO₂ system speciation at each spectral sampling point were calculated from the pH data, using version 1.05 of the CO₂SYN software (24), using the carbonate equilibrium constants calculated by Dickson and Millero (25) on the basis of a refit of Mehrbach's data. Of the CO₂SYN inputs, salinity (34.35), temperature (6 °C), and pressure (504.5 dbar) were measured in situ. The total alkalinity (TA; 2334 μmol/kg), initial [TCO₂] (2314 μmol/kg), silicate concentration (90.1 μmol/kg), and phosphate concentration (3.08 μmol/kg) were interpolated as a function

TABLE 2. Measured pH and Calculated CO₂ System Concentrations in the Raman Chamber at Each Spectral Acquisition

sample	T (°C)	pH (NBS)	[TCO ₂] (±std dev) (μmol/kg)	[CO ₂ *] (μmol/kg)	[HCO ₃ ⁻] (μmol/kg)	[CO ₃ ²⁻] (μmol/kg)
S0 (seawater)	5.97	7.708	2314 (2)	56	2210	48.0
S1	6.13	5.542	11050 (220)	8713	2336	0.3
S2	6.01	5.229	20330 (450)	17990	2340	0.2
S3	6.04	5.054	29320 (670)	26970	2343	0.1
S4	6.11	4.932	38090 (890)	35740	2346	0.1
S5	6.06	4.849	45640 (1070)	43290	2349	0.1
S6	6.02	4.766	54750 (1300)	52390	2352	0.1
S7	6.03	4.701	63350 (1510)	60990	2354	0.1
S8	6.10	4.646	71730 (1720)	69370	2357	0.0
S9	6.16	4.596	80270 (1930)	77910	2360	0.0
S10	6.18	4.550	88950 (2140)	86590	2363	0.0
S11	6.04	4.513	96630 (2330)	94270	2366	0.0
S12	5.98	4.459	109300 (2600)	106900	2370	0.0
S13	5.98	4.422	119300 (2900)	116900	2373	0.0
S14	5.98	4.391	128300 (3100)	125900	2376	0.0
S15	5.98	4.359	137900 (3400)	135500	2379	0.0

of σ_{θ} (27.06) from the WOCE P17N Station 10, 1993 data. The initial seawater pH (7.708) was calculated on the basis of these values. We estimate an uncertainty in the interpolated TA and initial [TCO₂] of $\pm 1 \mu\text{mol/kg}$, giving an estimated uncertainty in the initial pH of ± 0.006 . This uncertainty is propagated through as an estimated uncertainty in [TCO₂] at each sample point, and is greater than the uncertainty due to a 1% error in the carbonate equilibrium constants K_1 and K_2 . The results of these calculations are given in Table 2.

Raman Signal: Spectral Processing. Spectral analysis was performed using GRAMS/AI data processing software (Thermo Electron Corp.). All spectra were smoothed using a single pass of the third-order Savitsky–Golay smoothing function, where the smoothing width was determined from the full width at half-maximum (fwhm_{min}) height of the narrowest peak requiring resolution (26):

$$\text{smoothing width} = 0.7(\text{fwhm}_{\text{min}})/Y \quad (2)$$

where Y is the data resolution of the spectrum ($\Delta\text{cm}^{-1}/\text{data point} = 0.3$).

A conservative fwhm_{min} of $\sim 7 \Delta\text{cm}^{-1}$ was used for the low-wavenumber region ($0\text{--}2140 \Delta\text{cm}^{-1}$). In the high-wavenumber region ($2140\text{--}4400 \Delta\text{cm}^{-1}$), an fwhm_{min} of $70 \Delta\text{cm}^{-1}$ was used, equal to the width of the narrowest peak in the water stretching band when deconvolved to five overlapping Gaussian peaks. Both the low- and high-wavenumber regions were baseline corrected using a two-point linear fit to the data.

The peak position (i.e., Raman shift), height, fwhm, and area were determined using the GRAMS/AI peak-fitting routine with a Gaussian peak shape. The spectra were integrated from 920 to 1040 Δcm^{-1} (sulfate), from 1200 to 1475 Δcm^{-1} (CO₂ peaks and reference diamond), and from 2700 to 3900 Δcm^{-1} (water stretching band).

The intensity of Raman scattering can be written in simple form as

$$R = IKP\sigma C \quad (3)$$

where R is the Raman peak area, I is the laser intensity, K includes instrument parameters such as optical transmission and collection efficiency, P is the sample path length, σ is the Raman cross-section or scattering efficiency of the species under investigation, and C is the concentration per unit volume (27). As parameters such as K and P may differ in the

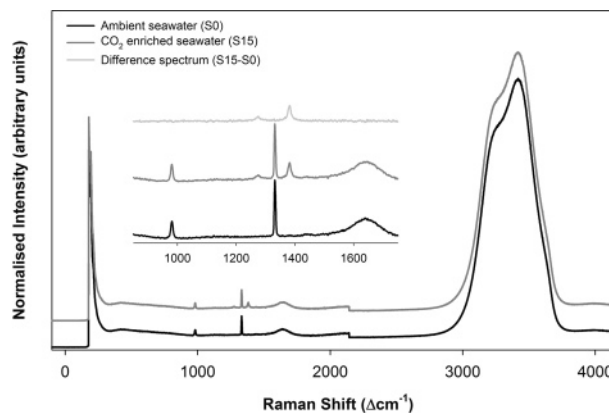


FIGURE 4. Raman spectra of seawater (black) and CO₂-enriched seawater (dark gray). The high-wavenumber region contains the high-intensity water stretching band (3000–3600 Δcm^{-1}). The inset shows the expanded low-wavenumber region containing the SO₄²⁻ ν_1 peak (981 Δcm^{-1}), the CO₂ Fermi dyad (1274 and 1382 Δcm^{-1}), the reference diamond peak (1332 Δcm^{-1}), and the water ν_2 peak (1640 Δcm^{-1}). The difference spectrum (light gray, S15 – S0) shows only the CO₂ Fermi dyad.

collection of separate spectra, an internal reference standard is required. For this experiment, all spectra were normalized to a constant area under the water stretching band. The entire spectrum was multiplied by the normalization factor N :

$$N = X/R_{\text{H}_2\text{O}} \quad (4)$$

where X is an arbitrary constant and $R_{\text{H}_2\text{O}}$ is the Raman peak area of the water stretching band for that spectrum. If we then consider eq 1 for both an unknown sample peak and the water stretching band, we obtain the following equations:

$$R_{\text{unknown}}^* = NIKP\sigma_{\text{unknown}}C_{\text{unknown}} \quad (5)$$

$$R_{\text{H}_2\text{O}}^* = X = NIKP\sigma_{\text{H}_2\text{O}}C_{\text{H}_2\text{O}} \quad (6)$$

where R^* indicates the normalized peak area. As R_{unknown} and $R_{\text{H}_2\text{O}}$ are collected simultaneously, the term $NIKP$ is equal in eqs 3 and 4, and the following relationship can be obtained:

$$R_{\text{unknown}}^* = A(C_{\text{unknown}}/C_{\text{H}_2\text{O}}) \quad (7)$$

where A is constant across all spectra and equal to

$$A = R_{\text{H}_2\text{O}}^*(\sigma_{\text{unknown}}/\sigma_{\text{H}_2\text{O}}) \quad (8)$$

Thus, the normalized area of any unknown Raman peak is directly proportional to the ratio of the concentration of the unknown species to the concentration of water.

Raman Spectra of Seawater and CO_{2(aq)}. The Raman spectra of ambient seawater (S0) and CO₂-enriched seawater (S15) are shown in Figure 4. The characteristic seawater peaks are due to the symmetric stretch of the sulfate ion (SO₄²⁻; $\nu_1 \approx 981 \Delta\text{cm}^{-1}$), and the water bending ($\nu_2 \approx 1640 \Delta\text{cm}^{-1}$) and stretching (3000–3800 Δcm^{-1}) modes. The water stretching band consists of a complex profile of several broad and overlapping peaks, where the relative intensity of these peaks is strongly dependent on the temperature and ions in solution (28, 29). No apparent difference in the shape of this band was seen between the spectra, consistent with the constant temperature of the experiment, and the small change in salinity (~ 1 unit overall; 10) due to dilution of seawater by the addition of a molecular species (TCO₂ is dominantly added as CO₂*; see Table 2), where the water:ion ratio remains unchanged. In the CO₂-enriched spectrum, the two additional

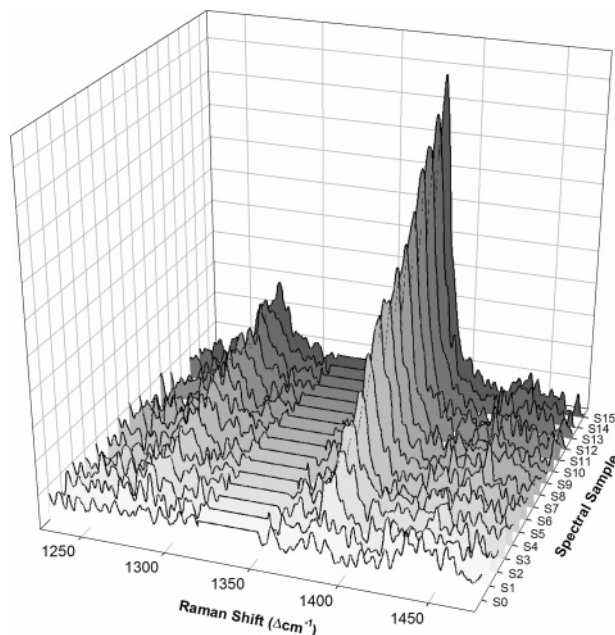


FIGURE 5. Raman spectra of the CO₂ Fermi dyad region for all samples (S0–S15). The diamond peak has been removed for clarity by setting the region from 1315 to 1350 Δcm⁻¹ to 0 (baseline). The CO₂ peaks are first observed in S2, where the increase in peak intensity from S2 to S15 as the seawater becomes progressively enriched in CO₂ can be clearly seen.

peaks of the CO₂ Fermi dyad (~1274 and ~1382 Δcm⁻¹), which result from a Fermi resonance between the 2 ν₂ and ν₁ peaks of the CO₂ molecule (3), are observed to either side of the reference diamond peak (~1332 Δcm⁻¹). Close examination of the low-wavenumber region reveals that no additional peaks are observed in any spectrum, and this was confirmed by obtaining difference spectra (S_{X,diff} = S_X - S₀). The difference spectrum for S15 is shown in the inset of Figure 4.

The low-wavenumber spectral region containing the CO₂ Fermi dyad for samples S0–S15 are displayed in stacked mode in Figure 5. The in-growth of CO₂ as dissolution progresses from ambient seawater (S0) to the most TCO₂ enriched sample (S15) can be clearly seen. The Raman peak position, height, and normalized area for the CO₂ peaks are presented in Table 3. The position of these peaks is relatively constant, with the smaller, low-wavenumber peak occurring at 1274.2 ± 0.9 Δcm⁻¹ (peak 1) and the larger, high-wavenumber peak at 1381.6 ± 0.3 Δcm⁻¹ (peak 2). Replicate measurements of S15 give an estimated precision in the normalized peak area of ±9% for peak 1 and ±2% for peak 2. The higher variation observed in both the position and normalized area of the first peak is attributed to an increased uncertainty due to the comparatively low peak intensity. The peak positions measured here agree well with previously published values for solution-phase CO₂ (1276 and 1384 Δcm⁻¹; 12), although there would appear to be a small decrease in peak frequency (~2 Δcm⁻¹) from the solution phase at 5 atm to the solution phase at 50 atm.

Combined pH and Raman Results and Raman Detection Limits. The integrated Raman peak areas for the CO₂ Fermi dyad (R_{p1}^* and R_{p2}^*) are plotted against the [CO₂*] determined from pH measurements in Figure 6. The area under the CO₂ peaks should be linearly related to the concentration ratio of aqueous CO₂ to H₂O (eq 7). However, the decrease in water concentration (due to dilution by CO₂*) is small, and may be considered negligible when compared to the large increase in [CO₂*] (Δ[H₂O] << Δ[CO₂*]). We therefore assume R_{p1}^* and R_{p2}^* are directly proportional to [CO₂*]. An excellent linear

TABLE 3. Measured Raman Peak Characteristics for the CO₂ Fermi Dyad

spectral sample	[CO ₂ *] (μmol/kg)	peak 1		peak 2	
		center X (Δcm ⁻¹)	area R _{p1} [*]	center X (Δcm ⁻¹)	area R _{p2} [*]
S0 (seawater)	56	nd	nd	nd	nd
S1	8710	nd	nd	nd	nd
S2	17990	1273.6	300	1381.3	1096
S3	26970	1274.2	442	1382.4	1683
S4	35740	1275.3	779	1381.1	2359
S5	43290	1276.1	807	1381.6	2827
S6	52390	1273.4	1172	1381.8	3680
S7	60990	1274.0	1516	1381.8	5226
S8	69370	1274.8	1647	1381.7	5463
S9	77910	1273.2	2234	1381.6	6189
S10	86590	1273.5	2085	1381.8	7342
S11	94270	1272.8	2636	1381.6	7790
S12	106900	1274.0	3042	1381.6	9026
S13	116900	1274.6	2978	1381.5	10385
S14	125900	1273.6	3690	1381.8	11363
S15a	135500	1274.5	3679	1381.5	12025
S15b	135500	1274.4	4102	1381.6	11608
S15c	135500	1274.7	3403	1381.5	11687

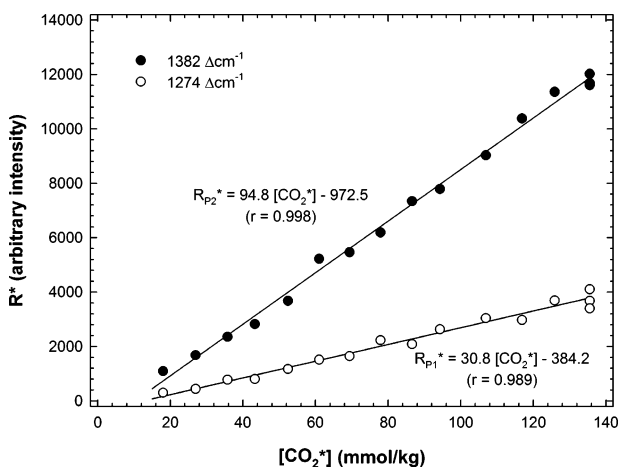


FIGURE 6. Normalized Raman peak areas for the CO₂ Fermi dyad plotted against calculated [CO₂*]. The model 2 linear fits (geometric mean regression) to the data are also shown.

relationship is observed between both R_{p1}^* and R_{p2}^* and [CO₂*], where model 2 linear regressions (geometric mean) yield the following relationships:

$$R_{p1}^* = 30.8C_{CO_2^*} - 384.2 \quad (9)$$

$$(r = 0.9887, \sigma_m = 1.23, \sigma_b = 113.0)$$

$$R_{p2}^* = 94.8C_{CO_2^*} - 972.5 \quad (10)$$

$$(r = 0.9977, \sigma_m = 1.70, \sigma_b = 155.8)$$

where $C_{CO_2^*}$ is in millimoles per kilogram. The excellent correlations observed clearly demonstrate that the novel application of in situ Raman spectroscopy provides quantitative data that compare very well with those of conventional pH sensing at equilibrium. These relationships indicate a detection limit, for this particular configuration and acquisition time, on the order of ~12.5 mmol/kg for peak 1 and ~10.3 mmol/kg for peak 2. This is consistent with the absence of CO₂ peaks in sample S1, where the CO₂* concentration was ~8.7 mmol/kg. The large negative y intercepts obtained in both regressions are most likely due to the peak-fitting

routine. In general, Raman peaks are best fit to a Lorentzian–Gaussian peak shape, where a high proportion of peak area is within the tails of the peak. However, for reasons of reproducibility, we chose to fit Gaussian peaks to the spectra, although this may result in a small underestimation of the total peak area.

We note that direct comparisons between detection of CO_2^* , HCO_3^- , and CO_3^{2-} should not be made due to different Raman scattering efficiencies of these species. Nevertheless, the detection limit determined here (~ 10 mM) significantly improves on previously reported Raman signal detection for the aqueous CO_2 system, and laboratory analysis has demonstrated that the current DORISS system allows direct detection (no advanced spectral processing) of 15 mM HCO_3^- , whereas the use of a new generation of advanced high-volume collection optics enables direct detection of 7 mM HCO_3^- (30). The present sensitivity of the DORISS instrument, although still too low for detection of oceanic background values, indicates that the application of the Raman technique appears very suitable for examination of natural deep-ocean volcanic CO_2 sources, where the CO_2 fluid signal is usually combined with elevated levels of other Raman-active species such as H_2S and CH_4 (11, 12).

Future Improvements. Our ultimate goal is to develop the use of in situ Raman spectroscopy to enable direct detection of ambient seawater CO_2 system speciation. To achieve this would require an improvement on current instrument sensitivity by a factor of 5–10, which should be readily attainable using well-known signal enhancement techniques such as the application of liquid core waveguides (LCWs).

Total reflection of light within an LCW increases the optical path length (i.e., the number of scattering centers sampled), and the application of LCWs has been widely demonstrated to greatly increase spectroscopic sensitivity by factors of 10–1000 (5–7). Song et al. (5) report a signal enhancement by a factor of ~ 20 for aqueous Na_2CO_3 using a 1 m Teflon-AF LCW and laser wavelength of 785 nm. Excitation at shorter wavelengths (e.g., DORISS laser wavelength of 532 nm) is expected to give significantly higher transmission efficiency in aqueous solution, leading to an effective higher enhancement of the Raman signal (5). Thus, it would appear that a 20-fold, or greater, improvement on current in situ Raman detection limits within the near future is realistic. If this is achieved, the Raman technique would allow direct detection of the individual components of the aqueous CO_2 system at natural background levels, in addition to observation of the extent of disequilibrium in CO_2 -enriched plumes emanating from either a sequestration experiment “disposal” site (10) or a natural seafloor vent site.

Dissolution Rate of Liquid CO_2 . The dissolution rate of liquid CO_2 can vary greatly with the vigor of mixing, which changes both the surface area exposed and the thickness of the diffusive boundary layer. In this experiment only slow mixing rates were intermittently applied, so any estimate will represent a low end member for the rate. We have made such a calculation as follows.

The $[\text{TCO}_2]$ (determined from pH measurements) in the measurement chamber at each sampling point, TM_S , is dependent on the $[\text{TCO}_2]$ for the previous sample point, TM_{S-1} , and the additional volume of CO_2 -enriched seawater transferred from the dissolution chamber. The $[\text{TCO}_2]$ of the seawater transferred from the dissolution chamber is considered to be the final concentration reached at the end of the previous dissolution step ($S-1 \rightarrow S$), TD_{S-1}^f . Fluid in the dissolution chamber is also replaced by less enriched fluid from the measurement chamber, such that the $[\text{TCO}_2]$ at the

start of the subsequent dissolution step ($S \rightarrow S+1$), TD_S^i , is reduced. These relationships are expressed in eqs 11 and 12,

$$\text{TD}_{S-1}^f = \frac{V_M \text{TM}_S - (V_M - E_S) \text{TM}_{S-1}}{E_S} \quad (11)$$

$$\text{TD}_{S-1}^i = \frac{(V_D - E_S)(V_M - E_S) \text{TD}_{S-1}^f + \text{TM}_{S-1}}{V_D} \quad (12)$$

where V_M is the volume of the measurement chamber (~ 5000 mL) and V_D is the volume of seawater in the dissolution chamber, assumed to be equal to the total volume minus the volume of liquid CO_2 (~ 4420 mL). E_S is the volume of fluid exchanged between the measurement and dissolution chambers prior to each sampling point, S , and can be accurately determined from the flow rate multiplied by the length of the exchange step. As a first approximation, we treat this transfer as occurring instantaneously at the midpoint of the exchange (t_s), where the length of the dissolution step, Δt_s , is then $t_s - t_{s-1}$.

These data give a mean dissolution rate of 12.5 ± 2.1 mmol/min (1σ), where the uncertainty primarily reflects the assumption of instantaneous transfer (with zero re-entrainment of water into the return flow back to the Raman chamber, and no account for changes in the dissolution regime under dynamic and static conditions). Consequently, this result represents an approximation, where the true dissolution rate under conditions of steady flow is likely to be moderately faster. The internal diameter of the CO_2 chamber is 22.9 cm. Assuming a planar circular interface (area ~ 410 cm²), this corresponds to a dissolution rate of ~ 0.50 ($\mu\text{mol}/\text{cm}^2$)/s. This estimate is of the same order of magnitude as our previous determinations of the dissolution rate of CO_2 into seawater, both under static conditions at 3600 m water depth (1.7 ($\mu\text{mol}/\text{cm}^2$)/s; 31) and under dynamic conditions as a plume of liquid CO_2 droplets rise through the water column from 800 m depth (3.0 ($\mu\text{mol}/\text{cm}^2$)/s; 32).

The successful formation of highly CO_2 enriched seawater under controlled conditions at depth suggests that this fluid could be readily created in large quantity for oceanic perturbation experiments. The experiment we carried out took place well within the P – T conditions of CO_2 hydrate formation (8, 9), yet our design enabled us to carry out the work over several hours without interference from hydrate plugging of the system, or hydrate formation at the CO_2 –seawater interface, causing a sufficiently large barrier to the dissolution rate (33) that formation of a large volume of low-pH–high- $[\text{CO}_2]$ water was inhibited. This shows the importance of the injection technique in carrying out this class of work. If a high-velocity jet reactor is used (34) to force contact between droplets of CO_2 and water in the required 1:6 ratio, then a pastelike composite of CO_2 hydrate can be readily formed. In this case we placed the CO_2 injection point so that the inlet was kept immersed within the liquid CO_2 phase, where the very low solubility of water in CO_2 ensures that hydrate formation at the injection point did not occur.

Acknowledgments

We gratefully acknowledge the support of the David and Lucile Packard Foundation and of the U.S. Department of Energy, National Energy Technology Laboratory, under Contract De-FC26-00NT4092. We thank the captain and crew of the RV *Point Lobos* and the pilots of the ROV *Ventana* for their skilled assistance in making the fieldwork possible.

Literature Cited

- (1) Brewer, P. G.; Malby, G.; Pasteris, J. D.; White, S. N.; Peltzer, E. T.; Wopenka, B.; Freeman, J.; Brown, M. O. Development of a

- laser Raman spectrometer for deep-ocean science. *Deep-Sea Res., Part I* **2004**, *51*, 739–753.
- (2) Pasteris, J. D.; Wopenka, B.; Freeman, J. J.; Brewer, P. G.; White, S. N.; Peltzer, E. T.; Malby, G. Raman spectroscopy in the deep ocean: successes and challenges. *Appl. Spectrosc.* **2004**, *58*, 195A–208A.
 - (3) Nakamoto, K. *Infrared and Raman Spectra of Inorganic and Coordination Compounds, Part A: Theory and Applications in Inorganic Chemistry*; Wiley: New York, 1997.
 - (4) Davis, A. R.; Oliver, B. G. A vibrational-spectroscopic study of the species present in the CO₂-H₂O system. *J. Solution Chem.* **1972**, *1*, 329–339.
 - (5) Song, L.; Liu, S.; Zhelyaskov, V.; El-Say-Ed, M. A. Application of Liquid Waveguide to Raman Spectroscopy in aqueous solution. *Appl. Spectrosc.* **1998**, *52*, 1364–1367.
 - (6) Altkorn, R.; Malinsky, M. D.; Van Duyn, R. P.; Koev, I. Intensity considerations in liquid core optical fiber Raman spectroscopy. *Appl. Spectrosc.* **2001**, *55*, 373–381.
 - (7) Marquardt, B. J.; Vahey, P. G.; Synovec, R. E.; Burgess, L. W. A Raman waveguide detector for liquid chromatography. *Anal. Chem.* **1999**, *71*, 4808–4814.
 - (8) Brewer, P. G.; Friederich, G.; Peltzer, E. T.; Orr, Jr., F. M. Direct experiments on the ocean disposal of fossil fuel CO₂. *Science* **1999**, *284*, 943–945.
 - (9) Brewer, P. G.; Peltzer, E. T.; Friederich, G.; Aya, I.; Yamane, K., Experiments on the ocean sequestration of fossil fuel CO₂: pH measurements and hydrate formation. *Mar. Chem.* **2000**, *72*, 83–93.
 - (10) Brewer, P. G.; Peltzer, E. T.; Walz, P.; Aya, I.; Yamane, K.; Kojima, R.; Nakajima, Y.; Nakayama, N.; Haugan, P.; Johannessen, T. Deep ocean experiments with fossil fuel carbon dioxide: Creation and sensing of a controlled plume at 4 km depth. *J. Mar. Res.* **2005**, *63*, 9–33.
 - (11) Sakai, H.; Gamo, T.; Kim, E.-S.; Tsutsumi, M.; Tanaka, T.; Ishibashi, J.; Wakita, H.; Yamano, M.; Oomori, T. Venting of carbon dioxide-rich fluid and hydrate formation in Mid-Okinawa Trough backarc basin. *Science* **1990**, *248*, 1093–1096.
 - (12) Lupton, J.; Lilley, M.; Butterfield, D.; Evans, L.; Embley, R.; Olson, E.; Proskurowski, G.; Resing, J.; Roe, K.; Greene, R.; Lebon, G. Liquid Carbon Dioxide Venting at the Champagne Hydrothermal Site, NW Eifuku Volcano, Mariana Arc. *EOS, Trans. AGU* **2004**, *85* (47), Fall Meeting Suppl., Abstr. V43F-08.
 - (13) Shitashima, K. CO₂ supply from deep-sea hydrothermal systems. *Waste Manage.* **1997**, *17*, 385–390.
 - (14) Johnson, K. S. Carbon dioxide hydration and dehydration kinetics in sea water. *Limnol. Oceanogr.* **1982**, *27*, 849–855.
 - (15) Soli, A. L.; Byrne, R. H. CO₂ system hydration and dehydration kinetics and the equilibrium CO₂/H₂CO₃ in aqueous NaCl solution. *Mar. Chem.* **2002**, *78*, 65–73.
 - (16) Oliver, B. G.; Davis, A. R. Vibrational spectroscopic studies of aqueous alkali metal bicarbonate and carbonate solutions. *Can. J. Chem.* **1973**, *51*, 698–702.
 - (17) Abbott, T. M.; Buchanan, G. W.; Kruus, P.; Lee, K. C. Carbon-13 nuclear magnetic resonance and Raman investigations of aqueous carbon dioxide systems. *Can. J. Chem.* **1982**, *60*, 1000–1005.
 - (18) Frantz, J. D. Raman spectra of potassium carbonate and bicarbonate aqueous fluids at elevated temperatures and pressures: comparison with theoretical simulations. *Chem. Geol.* **1998**, *152*, 211–225.
 - (19) Brewer, P. G. Ocean chemistry of the fossil fuel CO₂ signal: The haline signal of “business as usual”. *Geophys. Res. Lett.* **1997**, *24*, 1367–1369.
 - (20) Caldeira, K.; Wickett, M. E. Anthropogenic carbon and ocean pH. *Nature* **2003**, *425*, 365.
 - (21) White, S. N.; Brewer, P. G.; Peltzer, E. T. Determination of gas bubble fractionation rates in the deep ocean by laser Raman spectroscopy. *Mar. Chem.*, in press.
 - (22) Tedesco, J. M.; Davies, K. L. Calibration of dispersive Raman process analyzers. *Proc. SPIE-Int. Soc. Opt. Eng.* **1999**, 3537, 200–212.
 - (23) Zheng, X.; Fu, W.; Albin, S.; Wise, K. L.; Javey, A.; Cooper, J. B. Self-referencing Raman probes for quantitative analysis. *Appl. Spectrosc.* **2001**, *55*, 382–388.
 - (24) Lewis, E.; Wallace, D. W. R. *Program Developed for CO₂ System Calculations*; ORNL/CDIAC-105; Carbon Dioxide Information Analysis Center, Oak Ridge National Laboratory, U.S. Department of Energy: Oak Ridge, TN, 1998.
 - (25) Dickson, A. G.; Millero, F. J. A comparison of the equilibrium constants for the dissociation of carbonic acid in seawater media. *Deep-Sea Res.* **1987**, *34*, 1733–1743.
 - (26) Wilson, P. D.; Polo, S. R. Polynomial filters of any degree. *J. Opt. Soc. Am.* **1981**, *71*, 599–603.
 - (27) Pelletier, M. J., Ed. *Analytical Applications of Raman Spectroscopy*; Blackwell Science Ltd.: Oxford, 1999; 478 pp.
 - (28) Walrafen, G. E.; Hokmabadi, M. S.; Yang, W.-H. Raman isosbestic points from liquid water. *J. Chem. Phys.* **1986**, *85*, 6964–6969.
 - (29) Terpstra, P.; Combes, D.; Zwick, A. Effects of salts on dynamics of water: A Raman spectroscopy study. *J. Chem. Phys.* **1990**, *92*, 65–70.
 - (30) Brewer, P. G.; Dunk, R. M.; White, S. N.; Peltzer, E. T.; Bowie, B.; Walz, P. M. First attempts at direct Raman detection of the oceanic carbonate system. *EOS, Trans. AGU* **2004**, Fall Meeting Suppl., Abstr. OS43B-0557.
 - (31) Dunk, R. M.; Peltzer, E. T.; Rehder, G.; Brewer, P. G. Dissolution rate of liquid CO₂ at 3600m depth as determined by pH measurements. *EOS, Trans. AGU* **2002**, Ocean Sciences Meeting Suppl., Abstr. OS51F-06.
 - (32) Brewer, P. G.; Peltzer, E. T.; Friederich, G.; Rehder, G. Experimental determination of the fate of rising CO₂ droplets in seawater. *Environ. Sci. Technol.* **2002**, *36*, 5441–5446.
 - (33) Rehder, G.; Kirby, S. H.; Durham, W. B.; Stern, L. A.; Peltzer, E. T.; Pinkston, J.; Brewer, P. G. Dissolution rates of pure methane hydrate and carbon dioxide hydrate in under-saturated seawater at 1000m depth. *Geochim. Cosmochim. Acta* **2004**, *68*, 285–292.
 - (34) Tsouris, C.; Brewer, P. G.; Peltzer, E.; Walz, P.; Riestenberg, D.; Liang, L.; West, O. R. Hydrate composite particles for ocean carbon sequestration: field verification. *Environ. Sci. Technol.* **2004**, *38*, 2470–2475.

Received for review June 20, 2005. Revised manuscript received October 11, 2005. Accepted October 19, 2005.

ES0511725